HHS Public Access

Author manuscript

Mater Sci Eng C Mater Biol Appl. Author manuscript; available in PMC 2020 March 01.

Published in final edited form as:

Mater Sci Eng C Mater Biol Appl. 2019 March ; 96: 10–19. doi:10.1016/j.msec.2018.10.073.

Effects of MgO, ZnO, SrO, and SiO_2 in Tricalcium Phosphate Scaffolds on *In Vitro* Genes Expression and *In Vivo* Osteogenesis

Dongxu Ke, **Solaiman Tarafder**, **Sahar Vahabzadeh**, and **Susmita Bose***

W. M. Keck Biomedical Materials Research Laboratory, School of Mechanical and Materials Engineering, Washington State University, Pullman, WA 99164-2920, USA

Abstract

β-tricalcium phosphate (β-TCP) is a versatile bioceramic for the use in many orthopedic and dental applications due to its excellent biocompatibility and biodegradability. Recently, the addition of additives to β-TCP has been proven to improve bone repair and regeneration, however, the underlying mechanism of enhanced bone regeneration is still unknown. In this study, strontium oxide (SrO), silica (SiO_2), magnesia (MgO), and zinc oxide (ZnO) were added to β-TCP for dense discs fabrication followed by *in vitro* evaluation using a preosteoblast cell line. Cell viability and gene expression were analyzed at day 3 and day 9 during the cell culture. MgO and SiO_2 were found to significantly enhance and expedite osteoblastic differentiation. A potential mechanism was introduced to explain the additive induced osteoblastic differentiation. In addition, *in vivo* characterizations showed that porous 3D printed MgO-SiO_2-TCP scaffolds significantly improved new bone formation after 16 weeks of implantation. This study shows beneficial effects of additives on osteoblastic viability and differentiation *in vitro* as well as osteogenesis *in vivo*, which is crucial towards the development of bone tissue engineering scaffolds.

Keywords

β-tricalcium phosphate; MgO, ZnO, SrO, and SiO_2; Gene expression; 3D printing; Osteogenesis

1. Introduction

β-tricalcium phosphate (β-TCP) is a widely used bone substitue material to initiate strong bonding between implants and host tissues as well as provide mechanical support for new bone growth elucidating its excellent osteoconductive nature. However, β-TCP is not osteoinductive and requires improvement for expediting bone growth. An effective approach is to add additives, such as silica (SiO_2), zinc oxide (ZnO), magnesia (MgO), and strontium oxide (SrO). The use of such additives allows for the alteration of physical, mechanical, and

*Corresponding author.

dissolution properties of CaPs.[1–4] In addition, *in vitro* and *in vivo* results have demonstrated that additives improve bone formation and biological responses of CaPs.[5–9]. It was reported that the presence of Si in calcium phosphate cement significantly enhanced the osteoblast differentiation *in vitro* till day 14.[7] Another study reported that the presence of Zn in calcium silicate coatings improved the viability, differentiation, and osteogenic gene expressions of rat bone marrow-derived pericytes as well as the new bone formation *in vivo* using the ovariectomised rabbit model. [9] However, mechanisms for additive-induced bone growth through cellular events are still unclear.

In the past decade, the exploration of bone biology has ushered biomaterials into a new era. With the discovery of bone growth factors, studies about their relationship with bone growth and possible signaling pathways were conducted to understand the mechanism of bone modeling and remodeling. Some of the most critical bone growth factors include bone morphogenetic protein 2 (BMP2), runt-related transcription factor 2 (RUNX2), osteoprotegerin (OPG), receptor activator of nuclear factor kappa-B ligand (RANKL), and vascular endothelial growth factor (VEGF). BMP2 is one major member of bone morphogenic proteins that has demonstrated an effective induction of osteoblastic differentiation. [10] RUNX2 is a key runt-related transcription factor responsible for osteoblastic differentiation. Osteoprotegerin (OPG) is a decoy receptor of RANKL. OPG and RANKL can form a complex which can block receptor activator of nuclear factor kappa B (RANK)/RANKL interaction that is responsible for inducing osteoclastogenesis.[11] Finally, VEGF is a cell secreted signal protein which can stimulate new blood vessel formation. These factors are involved in several signaling pathways, including RANKL–RANK pathway, which is important in the activation of osteoclastogenesis and bone remodeling, canonical Wnt pathway, which is associated with the anabolic regulation of bone construction, and BMP2–RUNX2 pathway, which regulates osteoblastic differentiation. [12–14]

Recognizing the importance of these growth factors allows us to better understand the effects of additives on bone growth and regeneration. In previous studies, we have shown the effects of different dopants on properties of TCP scaffolds, such as phase, mechanical strength, dissolution, and biological responses.[1,3] It was reported that the presence of MgO and SiO_2 in 3D printed TCP scaffold and plasma sprayed HA coating accelerated new bone formation *in vivo*.[15,16] We also reported the effects of SiO_2, SrO, MgO, and ZnO in β-TCP on osteoblastic RUNX2 expression *in vitro*.[17] In the current study, we expand our previous study and report the effects of SiO_2, SrO, MgO, and ZnO in β-TCP on osteoblastic BMP2, RUNX2, OPG, RANKL, and VEGF expressions using qRT-PCR. Based on the genes expression results, we choose to prepare 3D printed TCP and Mg-Si-TCP scaffolds for *in vivo* characterizations to further validate our *in vitro* results.

We hypothesize that additives should enhance osteoblastic differentiation by the expression of target gene markers *in vitro* and further improve the osteogenesis *in vivo.* In order to validate this hypothesis, pure TCP, Sr-TCP, Mg-TCP, Si-TCP, and Zn-TCP discs are fabricated by uniaxial pressing for *in vitro* evaluations using a preosteoblast cell line. Physicochemical properties of all discs are evaluated by X-ray diffractions and fourier transform infrared spectroscopy. The biological effects of these additives on osteoblastic

differentiation are evaluated by their cellular morphology, gene expression, and MTT assay after 3 and 9 days. Another set of porous TCP and Mg-Si-TCP scaffolds are prepared using 3D printing technology. These scaffolds are implanted into rat femoral defects for 8, 12, and 16 weeks to evaluate their biological properties *in vivo.* The schematic of this whole study is shown in Figure 1.

2. Materials and Methods

2.1 *In Vitro* Discs Preparation

All chemicals were purchased from Sigma-Aldrich (St. Louis, MO, USA) if not mentioned seperately. A solid state synthesis method was used to prepare β-TCP powder. Briefly, 2 moles of dicalcium phosphate and 1 mole of calcium carbonate were mixed by zirconia balls with a diameter 10 mm for 2 h using 5:1 milling media to powder weight ratio. The mixture was then heated to 1050°C for 24 h in order to synthesize β-TCP. Four different TCP-additive powders were prepared by making 20 g batches including the individual amount of additives (0.2g MgO for Mg-TCP, 0.1g SiO_2 for Si-TCP, 0.05g ZnO for Zn-TCP, 0.2g SrO for Sr-TCP) and β-TCP. The amount of each additive was based on optimization in previous studies. [1,3] 30 ml of anhydrous ethanol was added to each mixture and they were mixed by zirconia balls with a diameter 10 mm at 70 rpm for 6 h. Each TCP-additive powder was dried at 60 °Cfor 72 h as the final powder for *in vitro* discs preparation. Discs were fabricated in a steel mold (12 mm in diameter) by uniaxial pressing at 145 MPa followed by sintering at 1250 °C for 2 h.

2.2 Phase and Chemical Group Identifications

X-ray diffraction (XRD) was used to analyze the phase formation of sintered scaffolds with a step size of 0.05 degrees and count time of 0.5 seconds. The α-TCP percentage was calculated by the intensity of the 100% α-TCP peak divided by the sum of intensity from 100% α-TCP and 100% β-TCP. Pure TCP, Mg-TCP, Sr-TCP, Zn-TCP, and Si-TCP were scaned by Fourier transformed infrared spectroscopy (FTIR) to identify their chemical groups. Powders were grounded and placed on an ATR diamond crystal followed by scanning using an FTIR spectrometer (FTIR, Nicolet 6700, ThermoFisher, Madison, WI) in the range from 400 to 1200 cm^{-1}. The final graph was achieved by plotting transmittance percentage against wave number.

2.3 *In Vitro* Osteoblast Cell Culture

A standard autoclave cycle of 121 °C for 20 min was used to sterilize all scaffolds before cell culture. The cell line used in this study was human preosteoblast cell line (hFOB 1.19) from ATCC (Manassas, VA, USA). The cell medium used in this study was a solution containing Ham's F12 medium, Dulbecco's Modified Eagle Medium, 0.3 mg/mL Geneticin G418, 10 % fetal bovine serum, and 2 ml/L of Penicillin-Streptomycin-Amphotericin B Solution. 1 ml of cell medium was seeded on each sample with a concentration of 1×10^5 cells/ml. Samples were then incubated in a 34 °C and 5% CO_2/95% air environment. Cell medium was changed every three days.

2.4 Cellular Morphology

Samples were first fixed in 2 % paraformaldehyde/2 % glutaraldehyde in 0.1 M cacodylate buffer solution overnight at 4 °C. Then a post-fixation was conducted in 2 % osmium tetroxide (OsO_4) at room temperature for three hours. After fixation, each sample was dehydrated in an ethanol series (from 30 % to 100 %) and hexamethyldisilane (HMDS). Gold coating was conducted after the dehydration using a Technics Hummer V sputter coater at 10 milliamps for 6 min. After gold coating, cell morphology was able to be detected under FESEM.

2.5 Osteoblastic Viability Evaluation

A 3-(4,5-dimethylthiazol-2-yl)-2,5-diphenyl tetrazolium bromide (MTT) assay, containing 5 mg/ml MTT in filter sterilized phosphate-buffered saline, was used to analyze osteoblastic viability. MTT solubilizer was prepared using isopropanol, 10 % Triton X-100, and 0.1N HC1. Samples for MTT analysis were immersed in 100 μl MTT solution and 900 μl cell medium in an incubator at 34 °C. Samples were taken out after 2 h and 1 mL of MTT solubilizer was added to samples in order to dissolve formazan crystals. The measurement of absorbance was conducted by scanning supernatant from each sample in 96-well plates using a microplate reader at 570 nm. Three samples for each composition and three measurements for each sample were used to ensure reproducibility.

2.6 RNA Extraction and qRT-PCR

Aurum Total RNA Mini Kit from Bio-Rad (Hercules, CA, USA) was used for RNA extraction according to manufacturer recommended procedures. First, 20 μL strand cDNA was synthesized for each biological replicate by using iScript Advanced cDNA Synthesis Kit from Bio-Rad. The standard enzyme was then added for reverse transcriptase reaction under cyclic conditions on a CFX Connect Real Time PCR Detection System from Bio-Rad. Primer sets were prevalidated by using PrimePCR SYBR Green Assays purchased from Bio-Rad for BMP2, OPG, VEGF, RUNX2, and RANKL expressions, β-actin (ACTB) and ribosomal protein large P0 (RPLP0) were used as two housekeeping genes. Data were analyzed using Bio-Rad CFX Manager Software 3.0 software. Target gene expressions were normalized to housekeeping genes.

2.7 *In Vivo* 3D Printed Scaffold Preparation

Based on *in vitro* findings, we performed an *in vivo* study using porous 3D printed TCP control scaffolds and porous 3D printed TCP scaffolds with 0.5 wt. % SiO_2 and 1 wt. % MgO (Mg-Si-TCP) in the rat distal femoral model. Scaffolds were designed in a cylindrical shape with a diameter of 3.4 mm and a height of 5.2 mm. TCP control scaffolds and Mg-Si-TCP scaffolds were printed using a 3D printer (ExOne LLC, Irwin, PA, USA). Briefly, the powder bed needed to be filled with compacted powder prior to the printing process. Then a layer of powder was rolled from the feed bed to the build bed to initiate the layer-by-layer printing. After powder feeding, the commercially available binder for TCP was sprayed from the print head to the powder based on the design of 3D printed scaffolds. The extra binder was removed by the heater. This layer-by-layer process was continued until the whole scaffold was fabricated. To achieve the green 3D printed scaffolds, the powder on the build

bed were first transferred to an oven at 150 °C for 1.5 h. Then the compressed air was used to remove the loose powder on the printed structure. Finally, scaffolds were sintered at 1250 °C for 2 h in a furnace. Scaffolds were designed to have 350 μm interconnected pores, however, after sintering pore size shrank to 311 ± 5.9 and 268 ± 9.8 μm for pure TCP and Mg-Si-TCP scaffolds, respectively. Before surgeries, sintered scaffolds were autoclaved to prevent the contamination. The detailed process parameters and characterizations for this study can be found in previous studies. [19,15]

2.8 *In Vivo* Surgery Procedures

All rats were purchased from Simonsen Laboratories with an average body weight of 300 g (Gilroy, CA, USA). Four randomly chosen rats were used for each time points. Before surgery, a combination of isoflurane and oxygen was used to anesthetize rats. For individual rat, TCP control and Mg-Si-TCP scaffolds were implanted to 3 mm diameter cortical defects in the right femur and left femur, respectively. After implantation, they were housed with enough water and food in a room with a 12-hour cycle of light and dark for 8, 12 and 16 weeks. After each time point, they were euthanized by CO_2 and bone specimen with the implanted scaffolds were harvested for further analysis. All surgical procedures were performed based on an approved protocol by Institutional Animal Care and Use Committee (IACUC) of Washington State University.

2.9 Histomorphometric Analysis

Collected implants were fixed in the following solution order: 10 % neutral buffered formalin solution, 70 % ethanol, 95 % ethanol, 100 % ethanol, 1:1 ethanol-acetone mixture, and 100 % acetone. Then they were embedded in Spurr's resins followed by sectioning perpendicular using a low-speed diamond saw. After polishing, thin sections were stained with modified Masson Goldner's trichrome stain. Light microscope images were taken for histomorphometric analysis. Image J software was used to calculate new bone formation and osteon.

2.10 Statistical Analysis

Statistical analysis was conducted using one-way ANOVA method and two significant levels, *$p<0.05$ and **$p<0.01$. In order to ensure data accuracy, each composition also had three biological replicates and three technical replicates.

3. Results

3.1 Phase and Chemical Group Identifications

β-TCP is the dominant phase after sintering for all samples except Sr-TCP. The characteristic peaks of α-TCP and β-TCP in Figure 2 correspond well with JCPDS # 09-0348 for α-TCP and 09-0169 for β-TCP. The presence of MgO in TCP completely aviods the α-TCP phase formation after sintering. Pure TCP, Zn-TCP, Sr-TCP, and Si-TCP show 44.83%, 38.27%, 52.17%, and 36.17% of α-TCP respectively. For all compositions, they show similar peaks of antisymmetric P-O bending modes of phosphate group (v_4) β-TCP band shoulder, symmetric P-O stretching mode of phosphate group (v_1), and antisymmetric P-O stretching modes (v_3) as shown in Figure 2.

3.2 Cellular Morphology

Full coverage of the apatite formation is observed on pure TCP (Figure 3 (a) and (b)) and Zn-TCP (Figure 3 (e) and (f)) after 3 and 9 days. Cells are merged with apatite, but still form an excellent attachment with sample surface. Sr-TCP only has partial apatite formation, as shown in (Figure 3 (c) and (d)). For the surface area without the apatite, a single layer of cells is found at day 3. Osteoblasts show stretched multiple layers phenotype and increased cell density at day 9.

No apatite formation is found in Mg-TCP (Figure 4 (a) and (b)) and Si-TCP (Figure 4 (c) and (d)). A single layer of cells covers most of sample surface at day 3. Similar multiple layers phenotype and nearly total coverage of cells are detected at day 9.

3.3 Osteoblastic Viability

At day 3, the cell viability of Mg-TCP, Si-TCP, and Sr-TCP is significantly higher than pure TCP. After 9 days, all discs with additives show significantly higher cell viability than pure TCP, where Mg-TCP demonstrates the highest MTT level, as shown in Figure 5.

3.4 Target Gene Expression

At day 3, significant BMP2 upregulation was found on Mg-TCP and Si-TCP, as shown in Figure 6. OPG expression is upregulated significantly in all samples with additives, while no RANKL expression is detected in all samples at day 3. RUNX2 and VEGF expressions are also significantly elevated by the presence of additives, more notably by MgO and SiO_2.

At day 9, the BMP2 expression for Sr-TCP and pure TCP is negligible, but other compositions, especially Zn-TCP, have significantly higher BMP2 expression than pure TCP, as illustrated in Figure 6. Compared to BMP2 expression at day 3, all samples except Zn-TCP show downregulation at day 9. OPG expression for Sr-TCP is higher than pure TCP at day 9, while Mg-TCP, Zn-TCP, and Si-TCP show lower or comparable OPG expression compared to pure TCP at day 9. Pure TCP and Sr-TCP have increased OPG expression compared to day 3, while Mg-TCP and Si-TCP experience an OPG reduction and Zn-TCP has a similar OPG expression compared to day 3. Only Mg-TCP and Si-TCP show RANKL expression at day 9. The RUNX2 expression for pure TCP is negligible at day 9. RUNX2 expression is upregulated significantly in samples with additives compared to pure TCP. Comparing day 9 to day 3, the RUNX2 expression for Sr-TCP and Zn-TCP is upregulated, but RUNX2 expression is downregulated for pure TCP, Si-TCP, and Mg-TCP. All samples show lower VEGF expression compared to pure TCP except Mg-TCP. Schematic images to explain the results were shown in Figure 7 **and** 8.

3.5 *In Vivo* Histomorphometric Analysis

3D printed scaffolds after sintering and during surgery are shown in Figure 9a and 9b, respectively. At week 8, a large area of osteoid formation is observed for both TCP control and Mg-Si-TCP scaffolds, as shown in Figure 9c. New mineralized bone (NMB) formation also initiates at this time point showing an increase when comparing Mg-Si-TCP to TCP control, as shown in Figure 10a. When it comes to week 12, NMB formation dominates the bone remodeling. A significant increase of NMB is observed when comparing Mg-Si-TCP

to TCP control at week 12. At week 16, a significant increase of NMB is observed for Mg-Si-TCP comparing to TCP control. Osteon formation is also detected in both compositions, but Mg-Si-TCP has significantly more osteon formation than TCP control after 16 weeks of implantation, as shown in Figure 10b.

4. Discussion

All scaffolds were sintered at 1250 °C for 2 h prior to the use *in vitro* or *in vivo.* They all showed major TCP phase without a significant peak shift which indicated the presence of additives did not have significant effects on the TCP structure, as shown in Figure 2. MgO prevents α-TCP phase formation, while SiO_2 and ZnO decrease the α-TCP phase formation, and SrO increases the α-TCP phase formation. Additives have effects on the final phase formation based on their charge and ionic radii. Sr^{2+}, Mg^{2+}, and Zn^{2+} have the same charge as Ca^{2+}, so they usually substitute into the Ca^{2+} site during sintering. The ionic radii for those additives are 1.13 Å, 0.99 Å, 0.74 Å, and 0.65 Å for Sr^{2+}, Ca^{2+}, Zn^{2+} and Mg^{2+} ions, respectively. When Sr^{2+} substitutes Ca^{2+}, considering the larger ionic radius of Sr^{2} , Sr^{2+} will reside further to the axis of the cluster than Ca^{2+} resulting in a weaker Sr–O bond in the Ca-O position. This should be the reason that Sr-TCP shows increased α-TCP. Conversely, Mg^{2+} and Zn^{2+} substitution can increase the bond energy by residing closer to the axis of the cluster than Ca^{2+}, which is supported by a complete absence or decrease of α-TCP formation, as shown in Figure 2.[1,20] The substitution of Si^{4+} might happen at the P^{5+} site, where its ionic charge is larger than Si^{4+}. It likely causes crystal defects, which is a plausible reason for the decrease of α-TCP phase. [21] Similar results regarding the effects of additives on β to α-TCP phase transition were also found in our previous studies. [3,22]

To fully understand the mechanism of additive-induced osteogenesis, a short-term *in vitro* study was first conducted to evaluate the effects of additives on osteoblastic viability and differentiation using preosteoblastic cell line. Osteoblastic differentiation can be separated into two stages: early stage and late stage. In the early stage, preosteoblasts first differentiate to immature osteoblasts and then to mature osteoblasts. [17] In the late stage, mature osteoblasts differentiate to osteocytes, bone lining cells or undergo apoptosis, as shown in Figure 7.

RANKL/OPG ratio is an indicator for the progress of osteoblastic differentiation and bone remodeling. [23] It only starts to increase in the late stage of osteoblastic differentiation. The absence of RANKL expression for all compositions at day 3 indicates that osteoblasts are in the early stage of osteoblastic differentiation, as shown in Figure 6. BMP2 is reported to potently induce the early stage of osteoblastic differentiation.[10,24] Therefore a significantly higher BMP2 expression in Mg-TCP and Si-TCP denotes their enhanced early osteoblastic differentiation compared to pure TCP. RUNX2 usually plays a stimulatory role in the early stage of osteoblastic differentiation, but acts as an inhibitor in the late stage of osteoblastic differentiation.[25] Accordingly, elevated RUNX2 expression at day 3 demonstrates that additives enhance the early stage of osteoblastic differentiation compared to pure TCP. OPG can enhance osteoblastic differentiation from preosteoblasts to mature osteoblasts. [26] Thus, increased OPG expression at day 3 shows the expedited osteoblast differentiation to mature osteoblasts by the presence of additives compared to pure TCP.

VEGF can improve osteoblastic viability in the early stage of osteoblastic differentiation as well as enhance angiogenesis in the late stage of osteoblastic differentiation.[27] The upregulation of VEGF at day 3 should be the result of enhanced viability by the presence of additives since osteoblasts are still in the early stage of osteoblastic differentiation.

When osteoblasts approach their late stage of osteoblastic differentiation, the upregulation of RANKL usually comes with a downregulation of OPG, or at least the lower induction of OPG, which is in favor of osteoclastogenesis.[28] For pure TCP, Zn-TCP, and Sr-TCP, they have no RANKL expression at day 9, which indicates that they are still in the early stage of osteoblastic differentiation, as shown in Figure 6. Therefore, significantly higher BMP2 expression for Zn-TCP at day 9 is beneficial to its early stage of osteoblastic differentiation. Mg-TCP and Si-TCP show RANKL expression at day 9 indicating osteoblasts are expedited to the late stage of osteoblastic differentiation, which is in line with our finding of OPG expression at day 3. We discover that BMP2 plays an inhibitory role in the late stage of osteoblastic differentiation just like RUNX2.[25] Hence, the downregulation of BMP2 and RUNX2 for Mg-TCP and Si-TCP at day 9 compared to day 3 represents an enhanced late stage of osteoblastic differentiation. The downregulation of RUNX2 was also reported in a previous study showing its inhibitory role in the late stage of osteoblastic differentiation.[17]

For osteoblastic viability, higher MTT shows that the presence of all additives enhances osteoblastic viability compared to pure TCP, as shown in Figure 5. Even though both Mg-TCP and Si-TCP are in the late stage of osteoblastic differentiation at day 9, the MTT for Si-TCP is found to be much lower than Mg-TCP. The higher RANKL/OPG ratio for Si-TCP indicates that there should be more mature osteoblasts reached their fully differentiated morphology than Mg-TCP.[29] It is likely due to the apoptosis that decreases the cell viability on Si-TCP. In addition, pure TCP shows a slight decrease of the cell viability at day 9 compared to day 3. It might be due to the appatite formation on the sample surface, which inhibits the dissolution of purple formazan, as shown in Figure 3.

Based on our *in vitro* results, Mg^{2+} and Si^{4+} are significantly beneficial to osteoblastic differentiation. One possible reason is their effects on the regulation of Ryanodine Receptors (RyRs) from RyR channel outside ER membrane during the ion exchange in ER, as shown in Figure 8.[30] Briefly, RyR channel is a voltage-dependent, which is responsible for releasing RyRs through internal $Ca^{2+}$for activation.[31–33] RyRs can stimulate internal stored Ca^{2+}release via receptor-operated channels (ROCs), which further influences CamKII and CaN.[30] CamKII and CaN will regulate osteoblastic differentiation through NF-κB and NFAT.[17] It was reported that NF-κB and NFAT were able to control BMP2 expression, which further regulated RUNX2 expression.[12,34,35] In the early stage of osteoblastic differentiation, the upregulation of RUNX2 can increase OPG expression and decrease RANKL expression. However, in the late stage of osteoblastic differentiation, RUNX2 has totally reverse control on OPG and RANKL expressions. It might be possilbe to assume that RUNX2 controls the osteoblast differenitaion thourgh OPG and RANKL expression, however, further studies still need to be performed to confirm this finding. During the activation of RyR channel, Si^{4+}might stimulate more internal calcium release than Ca^{2+} because it contains four positive charges instead of two. Mg^{2+} has smaller atomic size,

which might be easier for charges to activate RyR channel than Ca^{2+}. In both cases, increased internal calcium release is beneficial to calcium regulated genes for improving osteoblastic differentiation. Another possible reason is due to the different amount α-TCP phase formation after sintering when adding different additives. When adding MgO and SiO_2, they have less α-TCP phase after sintering and they also play significant role in cell material interactions *in vitro* and bone formation *in vivo*.

Based on our promising *in vitro* results for Mg-TCP and Si-TCP, porous 3D printed TCP and Mg-Si-TCP scaffolds are prepared for a long-term *in vivo* study using a rat distal femoral model. Osteoid, new mineralized bone (NMB), and osteon formation are analyzed for evaluating the effects of MgO and SiO_2 on osteogenesis *in vivo.* For their functional differences, osteoid is secreted by osteoblasts at the beginning of new bone formation process followed by mineralization into NMB with surrounding bone cells. Osteon, also known as the haversian system, is the fundamentally functional unit of compact bone with laminar structures. [36] Hence, through the evaluation of osteoid, NMB, and osteon formation, we should make a conclusion about the effects of additives on osteogenesis *in vivo*.

A large amount of osteoid formation is observed in both samples at week 8 indicating the excellent biocompatibility of TCP, as shown in Figure 9. NMB formation presents in both samples until 16 weeks of implantation, however, a higher NMB formation is found in Mg-Si-TCP compared to TCP control showing an improved osteogenesis by the presence MgO and SiO_2. as shown in Figure 10. In addition, the number of osteons formed within 3D printed Mg-Si-TCP scaffolds is significantly greater than that of TCP control, which further confirms the enhancement of osteogenesis by the presence of MgO and SiO_2. All our *in vivo* data also correlate previous results showing the effects of MgO and SiO_2 on enhancing osteogenesis. [15,16] Both short-term *in vitro* and long-term *in vivo* studies show promising results using MgO and SiO_2 for improving biological properties of TCP. Target gene expression also corresponds well with *in vivo* results, which helps in gaining a better understanding for the effects of additives on bone biology.

5. Conclusion

In this study, the effects of MgO, SrO, ZnO, and SiO_2 on biological properties of TCP are explored *in vitro* and *in vivo.* It is shown that the presence of MgO and SiO_2 can influence osteogenesis-related gene expressions, such as OPG, RANKL, BMP2, RUNX2, and VEGF *in vitro* in a way which is favorable to the different stages of osteoblastic differentiation. *In vivo* study also shows that porous 3D printed Mg-Si-TCP scaffolds have significantly enhanced osteogenesis compared to TCP control after 16 weeks of implantation, which correlates well with *in vitro* results. In addition, this research presents a potential mechanism for the effects of additives on regulating key bone growth genes during osteoblastic differentiation and is valuable for the further related research.

Acknowledgements

The authors would like to acknowledge funding from the National Institute of Health under the grant numbers 1R01AR066361.

References

[1]. Bandyopadhyay A, Bernard S, Xue W, Bose S, Calcium Phosphate-Based Resorbable Ceramics: Influence of MgO, ZnO, and SiO_2 Dopants, J. Am. Ceram. Soc 89 (2006) 2675–2688. doi: 10.1111/j.1551-2916.2006.01207.x.

[2]. Carbajal L, Serena S, Caballero A, Saínz MA, Detsch R, Boccaccini AR, Role of ZnO additions on the β/α phase relation in TCP based materials: Phase stability, properties, dissolution and biological response, J. Eur. Ceram. Soc 34 (2014) 1375–1385. doi:10.1016/j.jeurceramsoc. 2013.11.010.

[3]. Bandyopadhyay A, Petersen J, Fielding G, Banerjee S, Bose S, ZnO, SiO_2, and SrO doping in resorbable tricalcium phosphates: Influence on strength degradation, mechanical properties, and in vitro bone-cell material interactions, J. Biomed. Mater. Res. B Appl. Biomater 100 (2012) 2203–2212. doi:10.1002/jbm.b.32789. [PubMed: 22997062]

[4]. Ito A, Sogo Y, Yamazaki A, Aizawa M, Osaka A, Hayakawa S, Kikuchi M, Yamashita K, Tanaka Y, Tadokoro M, de Sena LÁ, Buchanan F, Ohgushi H, Bohner M, Interlaboratory studies on in vitro test methods for estimating in vivo resorption of calcium phosphate ceramics, Acta Biomater 25 (2015) 347–355. doi:10.1016/j.actbio.2015.07.040. [PubMed: 26232621]

[5]. Silva DF, Friis TE, Camargo NHA, Xiao Y, Characterization of mesoporous calcium phosphates from calcareous marine sediments containing Si, Sr and Zn for bone tissue engineering, J. Mater. Chem. B 4 (2016) 6842–6855. doi:10.1039/C6TB02255C.

[6]. Bose S, Tarafder S, Banerjee SS, Davies NM, Bandyopadhyay A, Understanding in vivo response and mechanical property variation in MgO, SrO and SiO_2 doped beta-TCP, Bone. 48 (2011) 1282–1290. doi:10.1016/j.bone.2011.03.685. [PubMed: 21419884]

[7]. Mestres G, Le Van C, Ginebra M-P, Silicon-stabilized α-tricalcium phosphate and its use in a calcium phosphate cement: Characterization and cell response, Acta Biomater 8 (2012) 1169–1179. doi:10.1016/j.actbio.2011.11.021. [PubMed: 22154863]

[8]. Ke D, Bose S, Doped tricalcium phosphate bone tissue engineering scaffolds using sucrose as template and microwave sintering: enhancement of mechanical and biological properties, Mater. Sci. Eng. C. 78 (2017) 398–404. doi:10.1016/j.msec.2017.03.167.

[9]. Yu J, Xu L, Li K, Xie N, Xi Y, Wang Y, Zheng X, Chen X, Wang M, Ye X, Zinc-modified Calcium Silicate Coatings Promote Osteogenic Differentiation through TGF-β/Smad Pathway and Osseointegration in Osteopenic Rabbits, Sci. Rep 7 (2017) 3440. doi:10.1038/ s41598-017-03661-5. [PubMed: 28611362]

[10]. Marie PJ, Debiais F, Haÿ E, Regulation of human cranial osteoblast phenotype by FGF-2, FGFR-2 and BMP-2 signaling, Histol. Histopathol 17 (2002) 877–885. [PubMed: 12168799]

[11]. Buckley KA, Fraser WD, Receptor activator for nuclear factor kappaB ligand and osteoprotegerin: regulators of bone physiology and immune responses/potential therapeutic agents and biochemical markers, Ann. Clin. Biochem 39 (2002) 551–556. [PubMed: 12564836]

[12]. Lian JB, Stein GS, van Wijnen AJ, Stein JL, Hassan MQ, Gaur T, Zhang Y, MicroRNA control of bone formation and homeostasis, Nat. Rev. Endocrinol 8 (2012) 212–227. doi:10.1038/nrendo. 2011.234. [PubMed: 22290358]

[13]. Williams BO, Insogna KL, Where Wnts went: the exploding field of Lrp5 and Lrp6 signaling in bone, J. Bone Miner. Res. Off. J. Am. Soc. Bone Miner. Res 24 (2009) 171–178. doi:10.1359/ jbmr.081235.

[14]. Del Fattore A, Teti A, Rucci N, Osteoclast receptors and signaling, Arch. Biochem. Biophys 473 (2008) 147–160. doi:10.1016/j.abb.2008.01.011. [PubMed: 18237538]

[15]. Bose S, Tarafder S, Bandyopadhyay A, Effect of Chemistry on Osteogenesis and Angiogenesis Towards Bone Tissue Engineering Using 3D Printed Scaffolds, Ann. Biomed. Eng (2016) 1–12. doi:10.1007/s10439-016-1646-y. [PubMed: 26620776]

[16]. Ke D, Robertson SF, Dernell WS, Bandyopadhyay A, Bose S, Effects of MgO and SiO_2 on Plasma-Sprayed Hydroxyapatite Coating: An in Vivo Study in Rat Distal Femoral Defects, ACS Appl. Mater. Interfaces. 9 (2017) 25731–25737. doi:10.1021/acsami.7b05574. [PubMed: 28752993]

[17]. Fielding GA, Smoot W, Bose S, Effects of SiO_2, SrO, MgO, and ZnO dopants in tricalcium phosphates on osteoblastic Runx2 expression, J. Biomed. Mater. Res. A. 102 (2014) 2417–2426. doi:10.1002/jbm.a.34909. [PubMed: 23946240]

[18]. Tarafder S, Balla VK, Davies NM, Bandyopadhyay A, Bose S, Microwave-sintered 3D printed tricalcium phosphate scaffolds for bone tissue engineering, J. Tissue Eng. Regen. Med 7 (2013) 631–641. doi:10.1002/term.555. [PubMed: 22396130]

[19]. Ke D, Bose S, Effects of pore distribution and chemistry on physical, mechanical, and biological properties of tricalcium phosphate scaffolds by binder-jet 3D printing, Addit. Manuf 22 (2018) 111–117. doi:10.1016/j.addma.2018.04.020.

[20]. Yin X, Calderin L, Stott MJ, Sayer M, Density functional study of structural, electronic and vibrational properties of mg- and zn-doped tricalcium phosphate biomaterials, Biomaterials. 23 (2002) 4155–4163. [PubMed: 12182317]

[21]. Sayer M, Stratilatov AD, Reid J, Calderin L, Stott MJ, Yin X, MacKenzie M, Smith TJN, Hendry JA, Langstaff SD, Structure and composition of silicon-stabilized tricalcium phosphate, Biomaterials. 24 (2003) 369–382. doi:10.1016/S0142-9612(02)00327-7. [PubMed: 12423592]

[22]. DeVoe K, Banerjee S, Roy M, Bandyopadhyay A, Bose S, Resorbable Tricalcium Phosphates for Bone Tissue Engineering: Influence of SrO Doping, J. Am. Ceram. Soc 95 (2012) 3095–3102. doi:10.1111/j.1551-2916.2012.05356.x.

[23]. Huang JC, Sakata T, Pfleger LL, Bencsik M, Halloran BP, Bikle DD, Nissenson RA, PTH differentially regulates expression of RANKL and OPG, J. Bone Miner. Res 19 (2004) 235–244. doi:10.1359/JBMR.0301226. [PubMed: 14969393]

[24]. Liu T, Gao Y, Sakamoto K, Minamizato T, Furukawa K, Tsukazaki T, Shibata Y, Bessho K, Komori T, Yamaguchi A, BMP-2 promotes differentiation of osteoblasts and chondroblasts in Runx2-deficient cell lines, J. Cell. Physiol 211 (2007) 728–735. doi:10.1002/jcp.20988. [PubMed: 17226753]

[25]. Komori T, Regulation of bone development and extracellular matrix protein genes by RUNX2, Cell Tissue Res 339 (2010) 189–195. doi:10.1007/s00441-009-0832-8. [PubMed: 19649655]

[26]. Yu H, de Vos P, Ren Y, Overexpression of osteoprotegerin promotes preosteoblast differentiation to mature osteoblasts, Angle Orthod 81 (2010) 100–106. doi:10.2319/050210-238.1.

[27]. Tombran-Tink J, Barnstable CJ, Osteoblasts and osteoclasts express PEDF, VEGF-A isoforms, and VEGF receptors: possible mediators of angiogenesis and matrix remodeling in the bone, Biochem. Biophys. Res. Commun 316 (2004) 573–579. doi:10.1016/j.bbrc.2004.02.076. [PubMed: 15020256]

[28]. Boyce BF, Xing L, Biology of RANK, RANKL, and osteoprotegerin, Arthritis Res. Ther 9 Suppl 1 (2007) S1. doi:10.1186/ar2165. [PubMed: 17634140]

[29]. Atkins GJ, Kostakis P, Pan B, Farrugia A, Gronthos S, Evdokiou A, Harrison K, Findlay DM, Zannettino ACW, RANKL expression is related to the differentiation state of human osteoblasts, J. Bone Miner. Res 18 (2003) 1088–1098. doi:10.1359/jbmr.2003.18.6.1088. [PubMed: 12817763]

[30]. Stathopulos PB, Seo M, Enomoto M, Amador FJ, Ishiyama N, Ikura M, Themes and Variations in ER/SR Calcium Release Channels: Structure and Function, Physiology. 27 (2012) 331–342. doi:10.1152/physiol.00013.2012. [PubMed: 23223627]

[31]. MacLeod RJ, Hayes M, Pacheco I, Wnt5a secretion stimulated by the extracellular calcium-sensing receptor inhibits defective Wnt signaling in colon cancer cells, Am. J. Physiol. Gastrointest. Liver Physiol 293 (2007) G403–411. doi:10.1152/ajpgi.00119.2007. [PubMed: 17463182]

[32]. Lanner JT, Georgiou DK, Joshi AD, Hamilton SL, Ryanodine Receptors: Structure, Expression, Molecular Details, and Function in Calcium Release, Cold Spring Harb. Perspect. Biol 2 (2010). doi:10.1101/cshperspect.a003996.

[33]. Van Petegem F, Ryanodine receptors: structure and function, J. Biol. Chem 287 (2012) 31624–31632. doi:10.1074/jbc.R112.349068. [PubMed: 22822064]

[34]. Cho HH, Shin KK, Kim YJ, Song JS, Kim JM, Bae YC, Kim CD, Jung JS, NF-kappaB activation stimulates osteogenic differentiation of mesenchymal stem cells derived from human adipose

tissue by increasing TAZ expression, J. Cell. Physiol 223 (2010) 168–177. doi:10.1002/jcp.22024. [PubMed: 20049872]

[35]. Koga T, Matsui Y, Asagiri M, Kodama T, de Crombrugghe B, Nakashima K, Takayanagi H, NFAT and Osterix cooperatively regulate bone formation, Nat. Med 11 (2005) 880–885. doi:10.1038/nm1270. [PubMed: 16041384]

[36]. Wei S, Siegal GP, Introduction, in: Atlas Bone Pathol, Springer New York, 2013: pp. 1–21. doi:10.1007/978-1-4614-6327-6_1.

Highlights

1. MgO and SiO_2 significantly enhance and expedite osteoblast differentiation *in vitro*.
2. SrO and ZnO improve osteoblast differentiation, but not as effective as MgO and SiO_2.
3. A potential mechanism is explained for additive induced osteoblastic differentiation.
4. MgO/SiO_2 significantly improve *in vivo* osteogenesis of 3D printed TCP scaffolds.

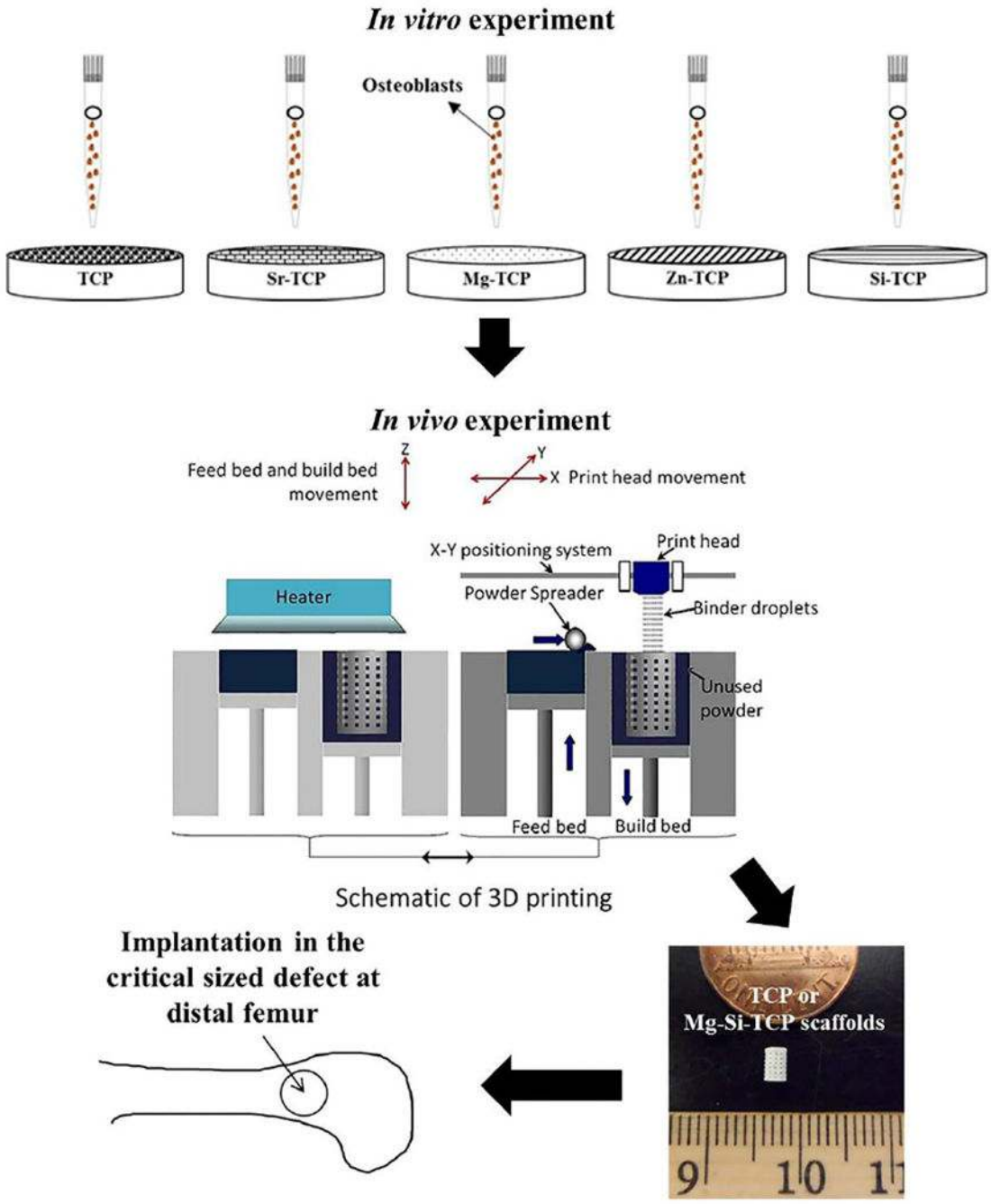

Figure 1.
The experimental design of this whole study. [18]

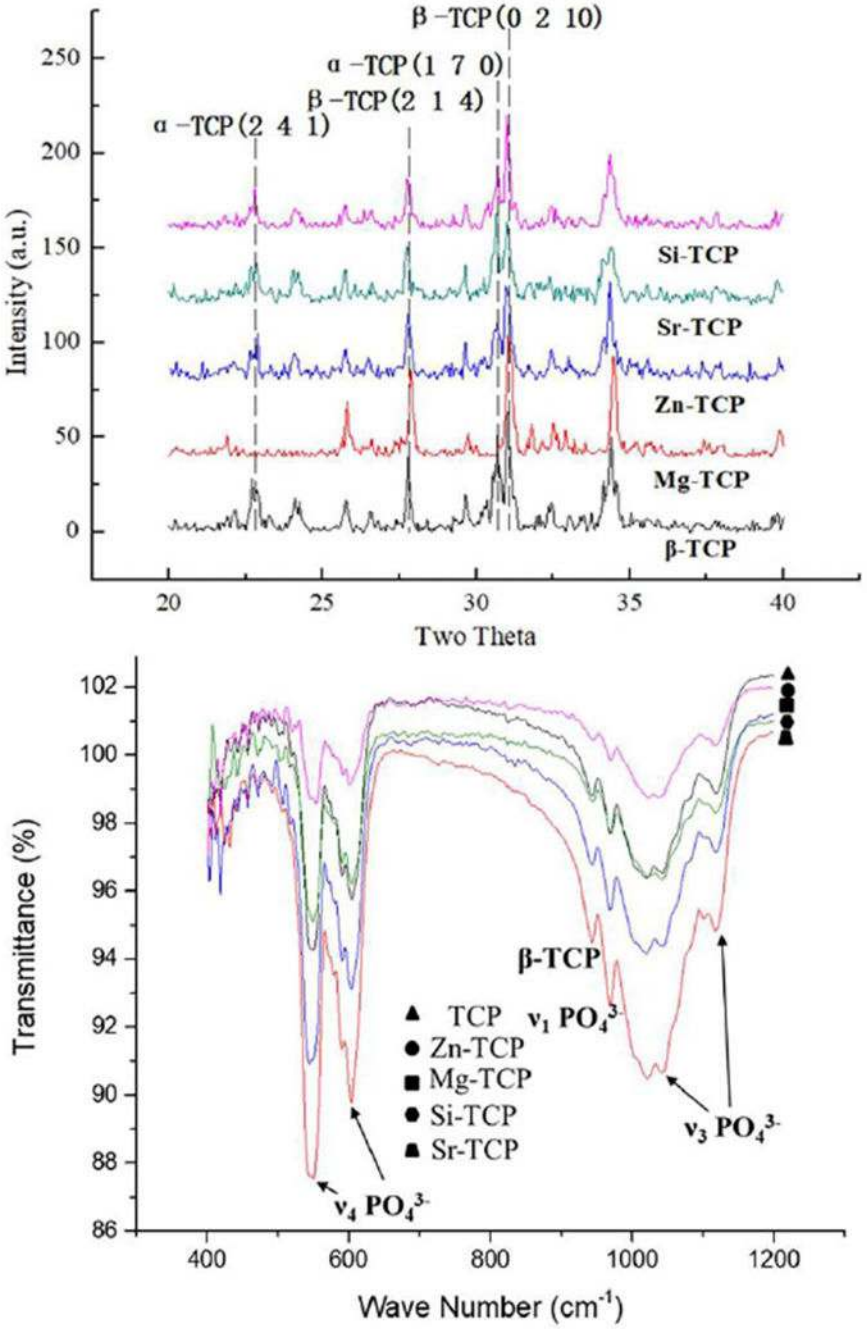

Figure 2.

Phase formation (A) and FTIR spectra (B) of pure TCP and TCPs with additives (MgO, SrO, ZnO, and SiO_2) after sintering at 1250 °C for 2 h showing characteristic TCP peaks. JCPDS #09-0348 and 09-0169 are used for identifying α-TCP and β-TCP, respectively.

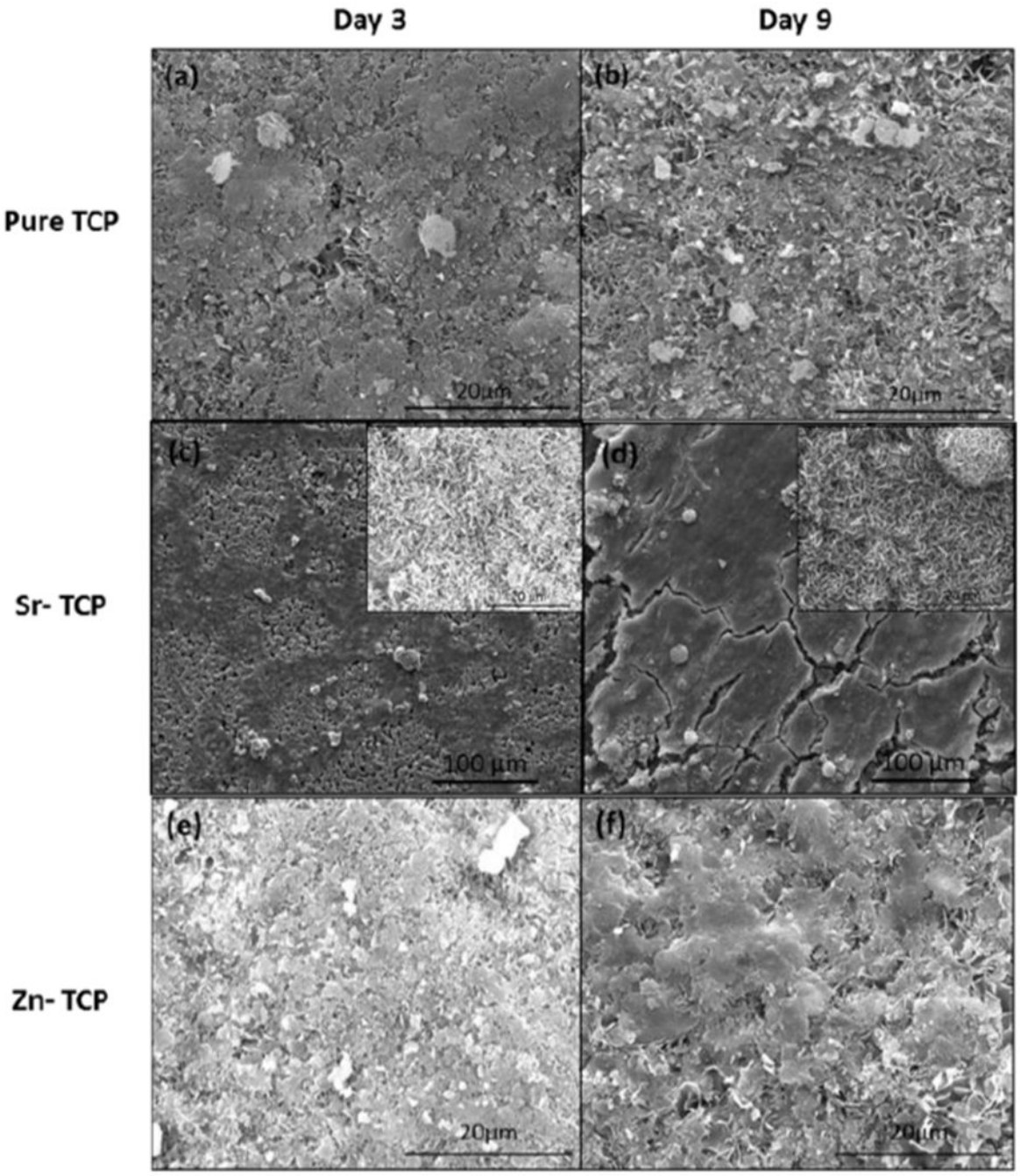

Figure 3.
Microstructure of pure TCP, Sr-TCP and Zn-TCP surfaces after 3 and 9 days of cell culture. For Sr-TCP, embedded images from (c) and (d) are images showing apatite formation in another location of sample surface.

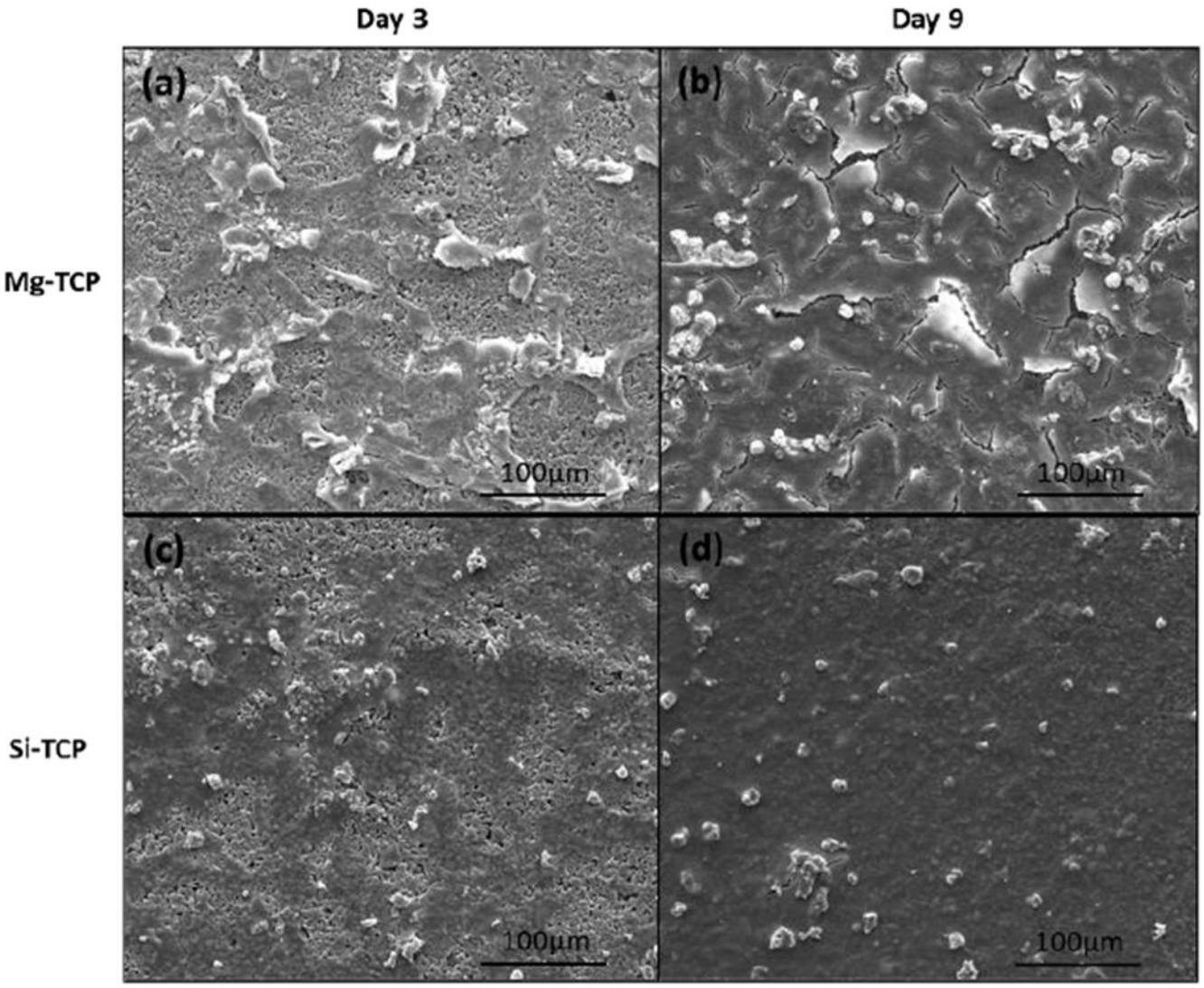

Figure 4.
Microstructure of Mg-TCP and Si-TCP surfaces after 3 and 9 days of cell culture.

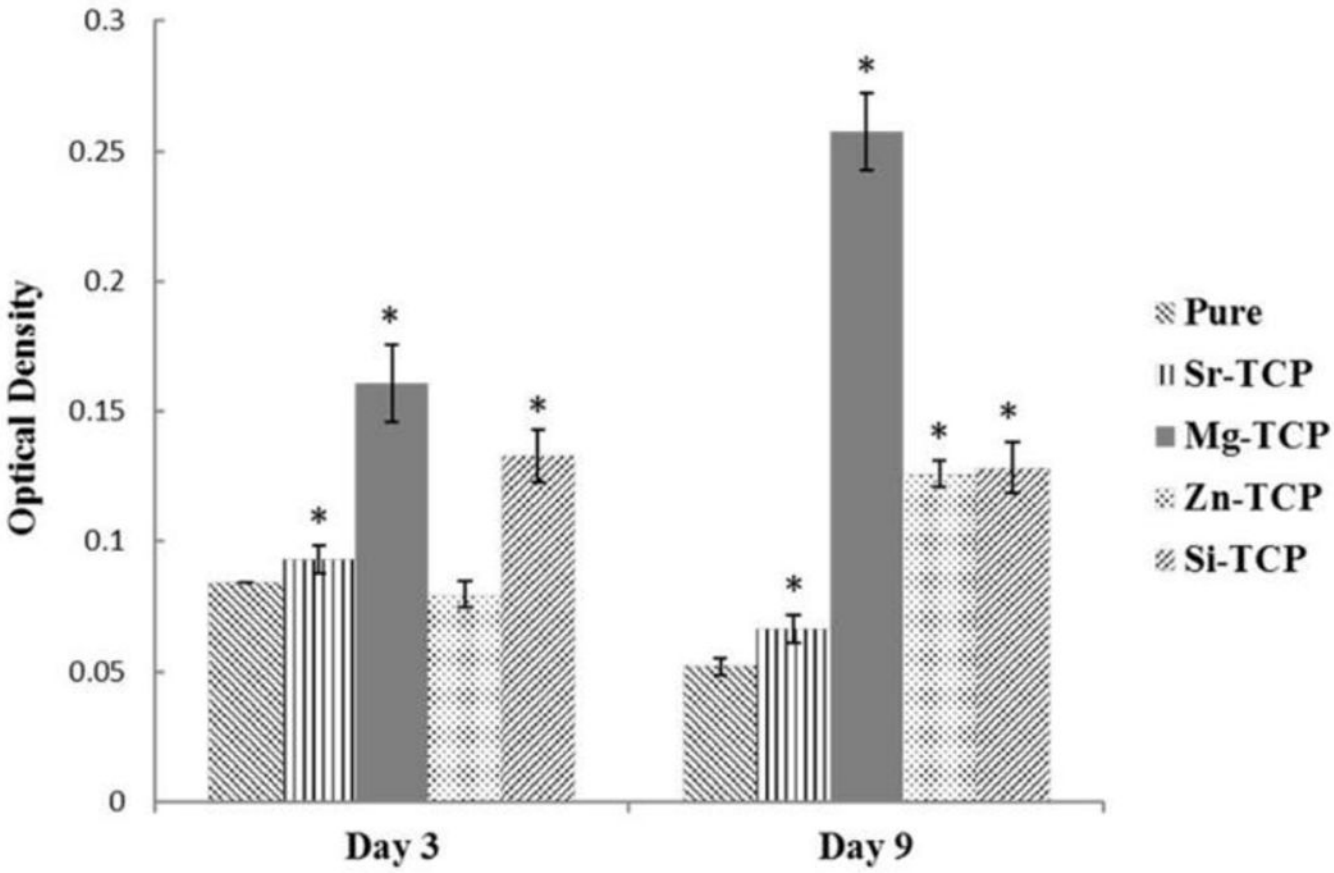

Figure 5.
MTT assay of pure TCP, Sr-TCP, Mg-TCP, Zn-TCP, and Si-TCP at day 3 and day 9 showing enhanced cell viability for doped TCP (*$p<0.05$, $n=3$).

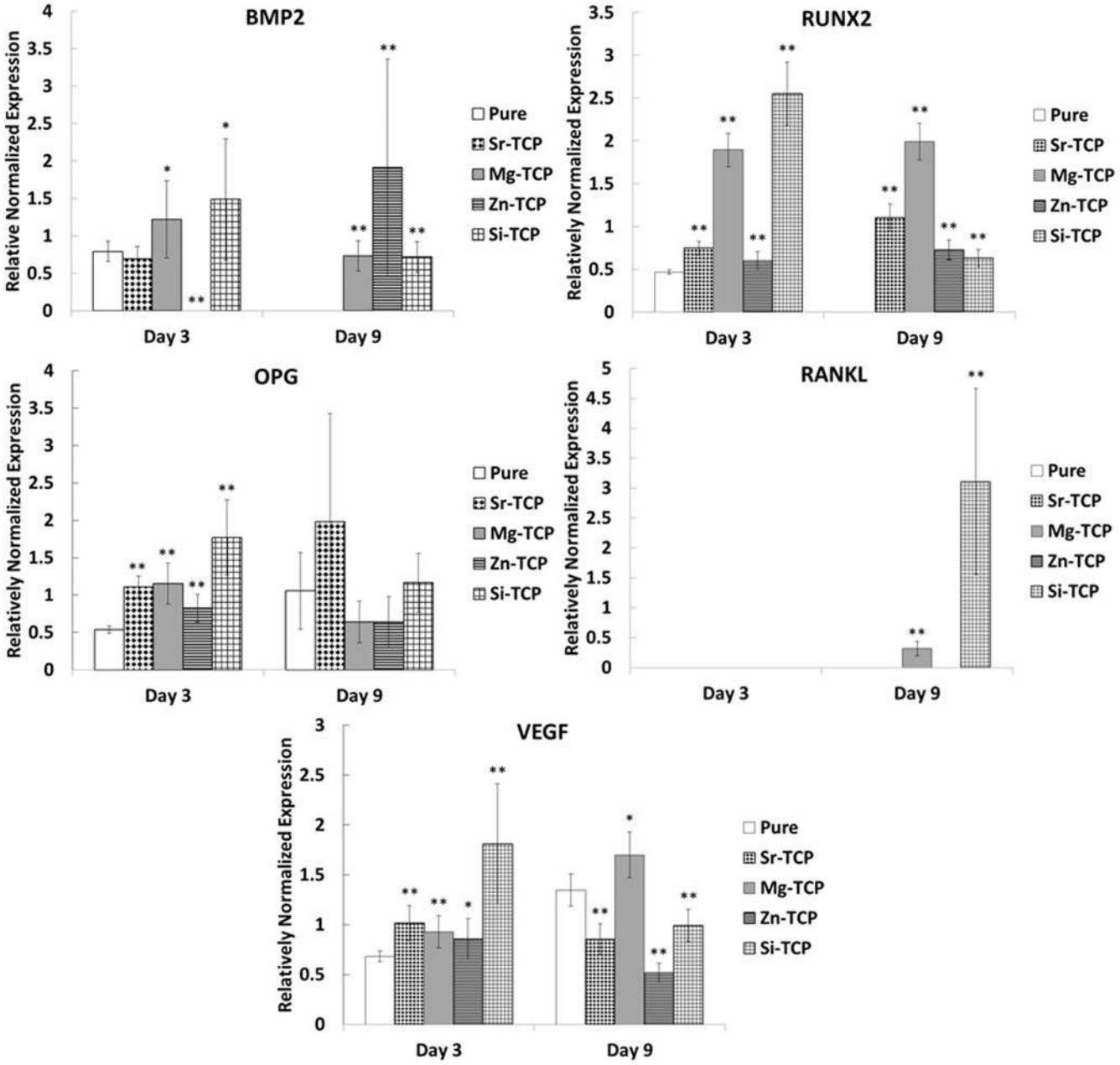

Figure 6.

BMP2, OPG, RANKL, RUNX2, and VEGF expression at day 3 and day 9. Pure, Sr, Mg, Zn and Si indicate pure TCP, Sr-TCP, Mg-TCP, Zn-TCP, and Si-TCP, respectively. All values are normalized by housekeeping genes (*p <0.05 and **p<0.01, where n=3).

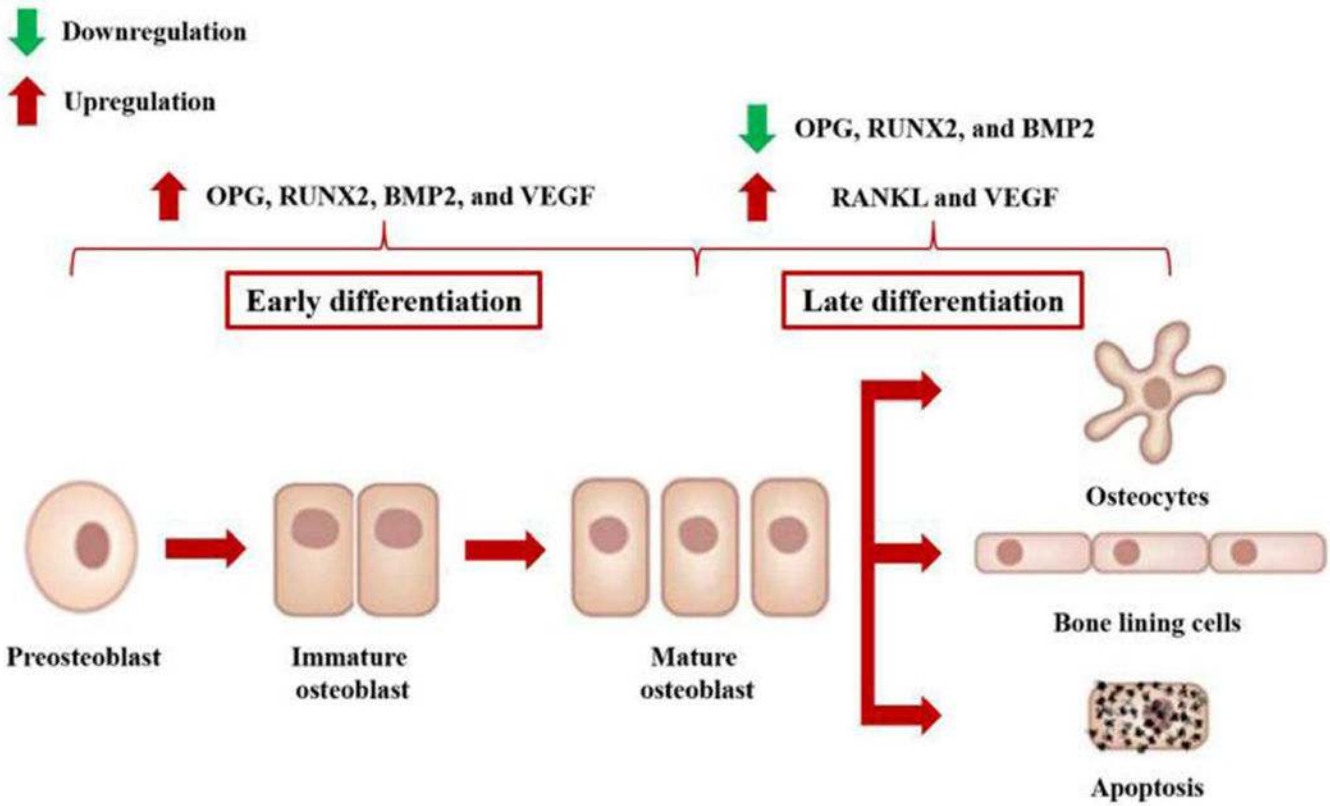

Figure 7.

The effects of OPG, RANKL, RUNX2, BMP2, and VEGF expressions on different stages of osteoblastic differentiation. Red up-arrows and green down-arrows indicate that the increase and decrease of related genes expressions can enhance different stages of osteoblastic differentiation, respectively.

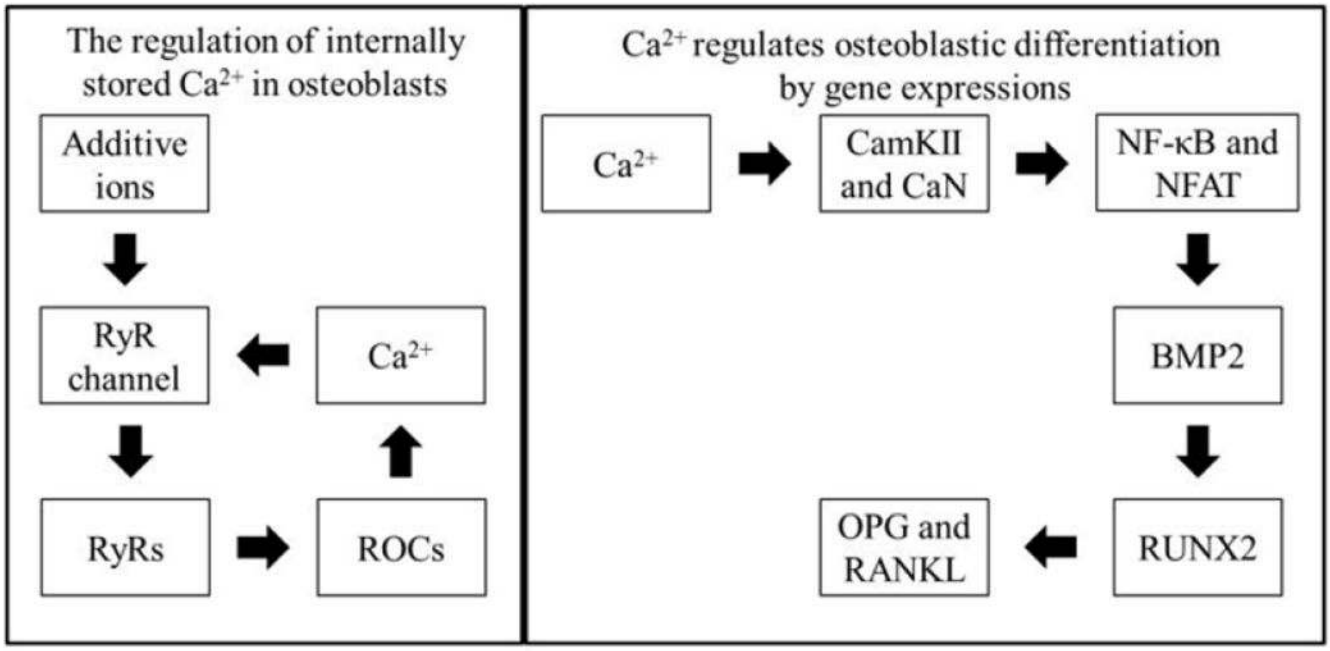

Figure 8.

Potential effects of additives on internally stored Ca^{2+} and the regulation of osteoblastic differentiation showing the presence of additives on the control of Ca^{2+} level, which further regulates osteoblastic differentiation through related genes expressions.

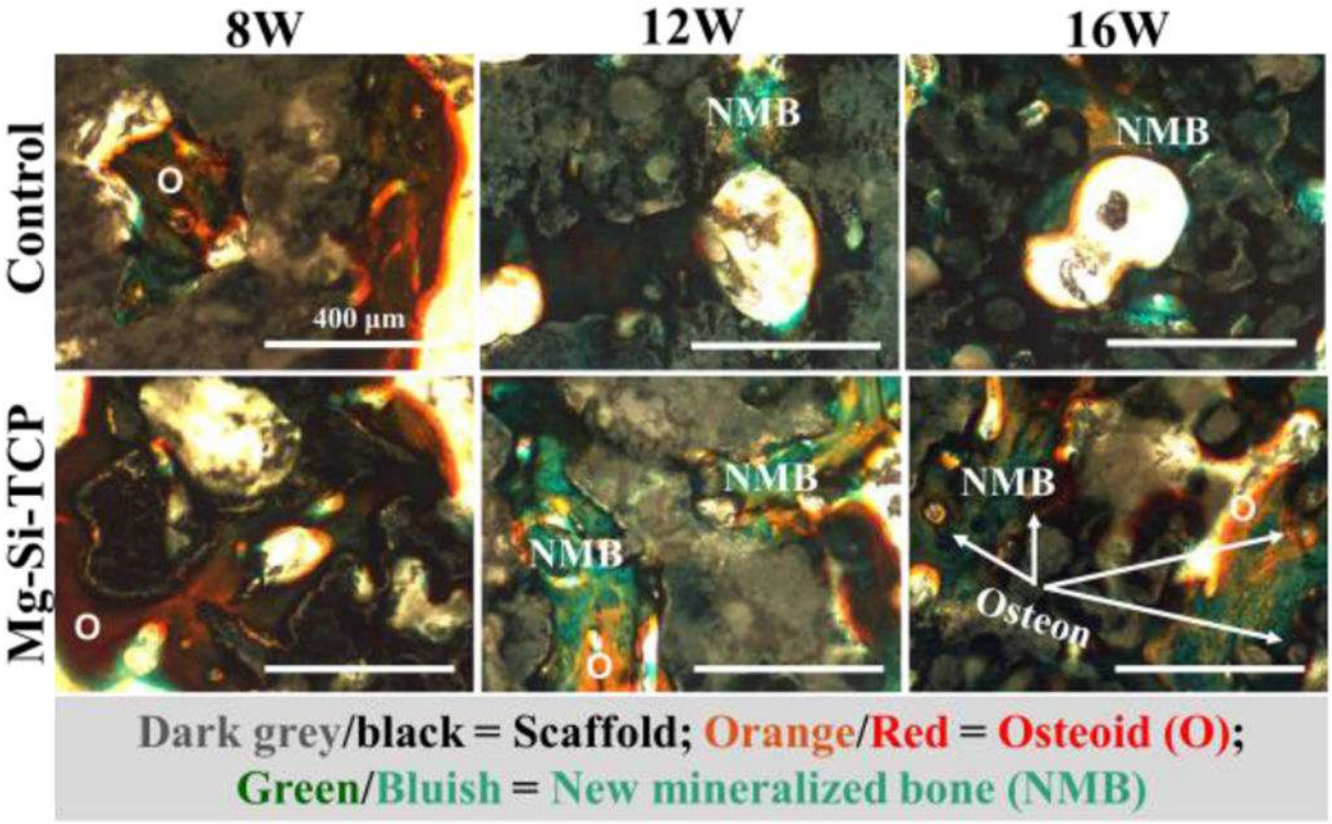

Figure 9.
Images of Masson Goldner's trichrome stained TCP control and Mg-Si-TCP scaffolds showing enhanced osteoid (O), new mineralized bone (NMB), and osteon formation for Mg-Si-TCP a rat distal femoral defect model after 8, 12, and 16 weeks.

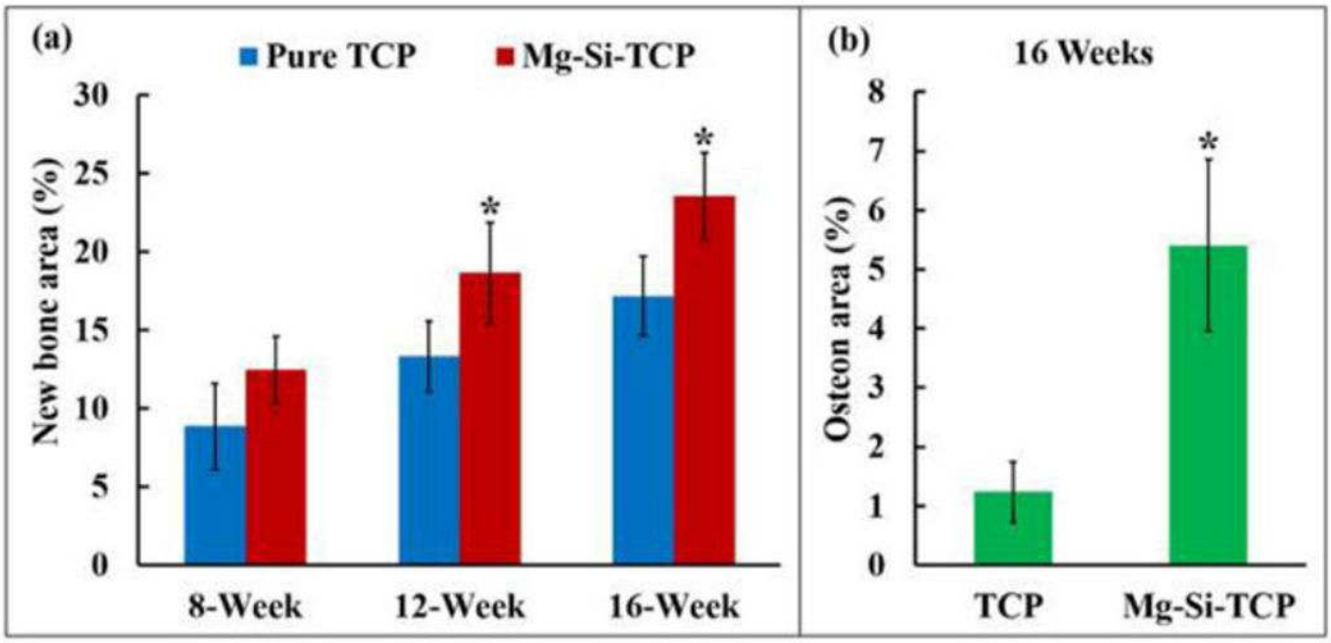

Figure 10.

Histomorphometric analysis of new mineralized bone (a) and osteon formation (b). New bone and osteon area percentage are achieved using new bone and osteon area divided by total area, respectively, showing the enhanced osteogenesis for Mg-Si-TCP (*$p < 0.05$, n=6).